BENTHAM SCIENCE

CrossMark

Current Medical Imaging

Content list available at: https://benthamscience.com/journals/cmir

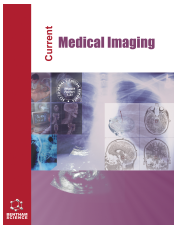

RESEARCH ARTICLE

Lung Cancer Detection from CT Images: Modified Adaptive Threshold Segmentation with Support Vector Machines and Artificial Neural Network Classifier

Sneha S. Nair[1,*], V. N. Meena Devi[1] and Saju Bhasi[2]

[1]*Department of Physics, Noorul Islam Centre for Higher Education, Kumarakovil, Kanyakumari District, Tamilnadu, India*
[2]*Department of Radiation Physics, Regional Cancer Centre, Thiruvananthapuram, Kerala, India*

Abstract:

Background:

The most difficult aspect of diagnosing lung cancer is early diagnosis. According to the American Cancer Society, each year, there are around 11 million newly diagnosed instances of cancer worldwide. Radiologists often turn to Computed Tomography (CT) scans to diagnose respiratory conditions, which can reveal if lung tissue remains normal or abnormal. However, there is an increased chance of inaccuracy and delay; therefore, radiologists are concerned with the physical segmentation of nodules.

Objective:

The objective of the research is to implement an advanced modified threshold segmentation and classification model for early and accurate detection of lung cancer from CT images.

Methods:

Using the Support Vector Machines (SVM) classifier as well as the Artificial Neural Network (ANN) classifier, the authors propose using Modified adaptive threshold segmentation as a segmentation approach for cancer detection. Here, Lung Image Database Consortium (LIDC) datasets, a collection of CT scans, are used as the video frames in an investigation to authorize the recitation of the suggested technique.

Results:

Both quantitative as well as qualitative analyses are used to analyze the segmentation function of the anticipated algorithm. Both the ANN and SVM classifiers used in the suggested technique for lung cancer diagnosis achieve world-record levels of accuracy, with the former achieving a 96.3% detection rate and the latter a 97% rate of accuracy.

Conclusion:

This innovation may have a major impact on the worldwide rate of lung cancer rate due to its ability to detect lung tumors in their earliest stages when they are most amenable to being avoided and treated. This method is useful because it provides more information and facilitates quick, precise decision-making for doctors diagnosing lung cancer in their patients.

Keywords: Accuracy, Classifier, Computed tomography, Diagnosis, Lidc dataset, Lung cancer.

Article History	Received: March 20, 2023	Revised: May 12, 2023	Accepted: June 13, 2023

1. INTRODUCTION

The importance of early lung cancer detection in improving patients' likelihood of living cannot be overstated. The time element is crucial in identifying irregularities in image features, especially cancer tumors like those seen in the lungs as well as the breast. So image-based processing approaches have lately gained popularity in several medical disciplines for contrast enhancement during pre-diagnosis as well as therapy stages. Lung cancer belongs to utmost dangerous illnesses, having a mortality rate higher than those of other diseases, such as colorectal and prostate cancers [1]. The rate of survival of patients can be improved by early diagnosis and intervention of lung potential nodules. Although

* Address correspondence to this author at the Department of Physics, Noorul Islam Centre for Higher Education, Kumarakovil, Kanyakumari District, Tamilnadu, India; E-mail: n.sneha85@gmail.com

CT scans are considered an important tool for early diagnosis and identification of lesions (potential nodules), radiologists face a difficult task in translating the broad measurements of thoracic tomographic images [2, 3]. As per the report, CT has a much greater rate of detecting possible nodules than simple radiography, with a disparity of 2 to 10 times [4]. However, analyzing a huge number of patient incidents is a daunting job for the radiologist, and it has a direct impact on the doctor's workload, which raises the risk of false detection and, as a result, increases the probability of error [5]. This necessitates the creation of a computational device capable of automatically detecting lesions and explaining their various effects and characteristics.

Unchecked cell proliferation in the lungs causes lung cancer, and discovering this early dramatically improves patients' chances of surviving the disease. New CT scanners have greatly improved the odds of early diagnosis, which has helped many people with lung tumors get treatment as soon as possible. The nodule seems to be a focal opacity in either a series form having a 3-30 mm diameter. Lung nodules range in size from very small to quite large [6]. The utilization of CT to capture images of the interior of a functioning human body has become common. Multiple X-ray beams are used to scan a human body part using the CT method. The opposite part of the body is equipped with X-ray detectors. Modern CT scanners can collect as many as 320 CT slices simultaneously. For regular chest protocols, a 2D slice thickness of 2.5 mm is typically used. Each of the 400 frames in a standard chest CT scan measures 512 by 512 pixels in size. Nodules that are too small to be seen on standard radiographs can now be seen with CT scans. The standard procedure for identifying lung nodules is for a specialist radiologist to carefully examine CT images. The existing problem regarding early detection is automatic lung nodule in Lung Image Database Consortium (LIDC) datasets. Image-based lung nodal recognition seems to be the primary standard for diagnosing respiratory illness. These problems could be fixed by designing an effective, minimally sized sequence of training image features. One of them had lung nodules that looked exactly like the one that was of interest to doctors. Typical steps include acquiring images, processing them, segmenting the lungs, identifying nodules, and minimization of false positives. The first thing that has to be done is to get a picture of the lungs. Many publicly accessible web datasets are now open to scrutiny. Some of them are the Lung Image Database Consortium (LIDC), Early Lung Cancer Action Programme (ELCAP), and the Reference Image Database for Evaluating Response to Therapy (RIDER). Several studies have indeed made use of researchers' access to private databases, which they have obtained through collaboration with hospitals [7, 8].

Lung segmentation preprocessing seems to be the second phase. By using preprocessing, CT image noise, as well as artifacts, can be reduced. Because images from various CT scanners might differ in size as well as brightness, preprocessing measures may be required before they can be utilized. Linear isotropic interpolation was used for data restoration by Cascio, Donato, *et al*. to generate consistent 3D spatial reconstruction [9]. Median screening for compression was performed by both Kim *et al*. and Soltanized *et al*. [10] before going on to architectural solutions for noise reduction [11]. Several studies have employed Gaussian filtering to get rid of artifacts, and this includes the studies by Pu *et al*., Gori *et al*., Wei *et al*., and Retico *et al*. [12 - 15]. Lung segmentation is the third stage. As the name suggests, “lung segmentation” is the process of initially isolating lung tissue from the surrounding muscle and fat. Lung division processes may be broken down into two broad categories: edge-based methods and thresholds and shapes [16]. Choi and Choi's method for quantifying lung capacity involves three stages: thresholding, segmentation refinement, and volumetric determination based on 3D-linked component coloring [17]. Keshani *et al*. used a multi-step process to divide the lungs into individual segments [18]. First, an adaptive fuzzy threshold method was used to collect binary images. It used to require two windows to create a seamless mask. After that, the lung surface area was calculated using active contour modeling. Kim *et al*.'s malleable prototype was used to delineate the lung regions. Using an active contour modeling approach, Belloti *et al*. [19, 20] demonstrated a larger lung region that had been segmented.

Moreover, at step 4, the nodule candidate looks to have been found. Choi and Choi matrices, which are based on the Hessian metric, can be used to find potentially useful node positions. To locate nodes, El-baz *et al*. developed a matching strategy based on an evolutionary algorithm [21]. First, a genetic approach was developed to regulate the center, and an appropriate radius was formed around the recognized picture. The second strategy was an algorithm based on template matching. The nodule was simulated by Cascio, Donato, and colleagues using a 3D mass-spring model. Suiyuan and Junfeng did thresholding in the study area, and the algorithm was applied to zero in likely nodule locations. Separating nodule shapes using dynamic programming was accomplished by Xu *et al*. [22], Aoyama, and Wang *et al*. [22 - 25]. Fan *et al*.'s 3D template matching approach is used to partition the nodules [26]. Kostic *et al*. used 3D morphological processing to classify lung nodules. The nodule candidate was found by Enquobahrie *et al*. [27], who utilized surface morphology analysis and volume occupancy analysis. Li *et al*. [28] created a rule-based classifier to recognize nodules. In their research on nodule detection, Kawata *et al*. [29] used k-means clustering with a linear discriminate (LD) classifier [30]. To locate nodules, Matsumoto *et al*. developed a novel filter called the quantized convergence index filter [31]. To identify potential nodule sites, Jia *et al*. and Fukano *et al*. respectively employed a morphological filter and a hessian-based detection strategy [32, 33]. Both Zhao *et al*. and Dehmeshki *et al*. used support vector machines (SVM) to classify nodules [34, 35].

The use of feature classifiers to decrease false positives is the fifth stage. SVM classifiers targeting node structure were created by Choi and Choi and Santos *et al*. [36]. To lessen the prevalence of false positives, El-baz *et al*. created a Bayesian supervised classifier. Rule-based classifiers were developed by Matsumoto *et al*. [37]. With their method, seven characteristics were determined for every potential nodule. Using these features, we determined cutoff values that were above where nodule candidates would be classified as actual nodules.

Effective medical image interpretation requires two

separate procedures: (1) recognizing attractive distinguishing patterns and (2) developing the possible link between image characteristics, clinical context, and probable therapies [38]. While the latter needs a thorough knowledge and comprehensive understanding of radioactivity occurrences and clinical aspects of disorders, the former means only a basic knowledge of the radioactivity occurrences and clinical aspects of illnesses [39]. The number of failures in medical data perception was induced by perceptual misunderstanding, according to a large–scale report on misconduct in radiology [40]. The normalization of observing environments, adequate preparation of the observers, accessibility of identical images and clinical evidence, multiple reporting, and image quantitative analysis are all strategies for minimizing perceptual errors [41]. Structured visual definitions based on radiology semantics are also a successful approach for enabling unequivocal interpretation of scanning signs, but they are still seldom used during routine practice [42]. When applied to the existing techniques, computerized image analysis and manipulation ought to be equipped to provide detailed, systematic, and repeatable data analysis [43]. As elevated image analysis based upon computer-generated image quantification as well as its clinical meaning resides in the possession of the reasonable eye, the abilities of computers and radiographers are considered to be very compatible. To overcome this issue, early detection and diagnosis are needed. Trial results of National Lung Screening show that early detection of lung tumors at lower-dose CT scans prevents 20% of fatalities [44]. However, CT evaluations for lung screening could become more common in the future. As a result, it produces more images that can be read by the radiologist on their own for error-free diagnosis interpretation. The image analysis tool that can be used is MATLAB. The Jpeg format is used for the image pixels. To isolate the cancer-affected sections, extensive pre-processing and differentiation are performed. Classification aims to check whether the object is normal or not. The tumor is recognized by counting all the pixels [45]. Multiple classifiers check the input image against those in a database; cancer is detected by tallying up the pixels. This feature extraction process is crucial in identifying and categorizing applications. Multiple classifiers for texture-based extracting features are used.

A fragmented tissue density region of the patient is used to make a lung cancer prediction [46]. First, a suspiciousness investigation is conducted, followed by classification is made to assess the degree of malignancy [47]. A method of extracting the features is used to analyze the data. The prediction regarding the development of lung cancer in patients requires performing a texture-based assessment [48]. To do this, a two-stage procedure is used. Initial processing involves training the system with a large sample of both cancerous and non-cancerous images. The second stage is testing, which involves analyzing and making predictions about the current image using the data for training [49]. Preprocessing is accomplished *via* smoothing, augmentation, and localization in a number of the current models. Segmentation techniques are used to perform the division [50, 51]. After that, we employ the GLCM to carry out the segmentation method. It is the job of the classifiers to make a prognosis regarding whether or not the nodule becomes cancerous. However, insufficient controls mean that not all targets are hit. With the suggested system, this problem will no longer exist.

This research article follows the outline below. The thresholding procedure is incorporated into the realization of the proposed investigation. The research aims to implement a modified threshold segmentation and classification model for early as well as accurate detection of lung cancer from CT images. On focussing the objective, we proposed employing the modified adaptive threshold segmentation (ADTM) technique in combination using a support vector machine (SVM) classifier as well as an artificial neural network (ANN) classifier to identify cancer. This research outcomes are obtained with the training and testing on the LIDC data sets. This technique employs a patch-based image subdivision strategy of nodule-specific size and shape information. Both the ANN and SVM classifiers used in the suggested technique for lung cancer diagnosis achieve world-record levels of accuracy.

2. PROPOSED METHODOLOGY

Filtration, classification, and extraction of features are the three phases of the recognition system. Lung cancer database-based images can be utilized as inputs, as the accuracy and effectiveness of tumor detection are enhanced by maintaining these stages. A modified adaptive thresholding method is used for segmentation, which helps to determine whether the input image has an infection occurred. Classifier helps to make detections more precise. MATLAB 2018a is used as a tool to apply the proposed methods for diagnostic imaging.

Fig. (**1**) depicts various phases of the suggested system that were applied to lung cancer detection. Lung Segmentation is done utilizing adaptive threshold, and feature extraction is utilized for extracting texture and shape features. Then classification of features is done using ANN and SVM. Every link inside an ANN-enabled ubiquitous input-output system is assigned a weight, and this model is what makes the network possible. Such a system has an input layer, an intermediate layer (or layers) as well as an output layer. To learn more about a computational model, the importance of a certain relation is tweaked. Changing the weight iteration procedure improves the network's efficiency. The weighted number of inputs activates neurons in a neural network. The stimulation output is processed *via* the transfer function, which results in a single neuron output. This output signal causes non-linearity in the network. Throughout the training, this network's accuracy is improved by adjusting the transmission rates of its interconnected nodes. Furthermore, an SVM classifier is employed for making a prognosis regarding whether or not the nodules are cancerous.

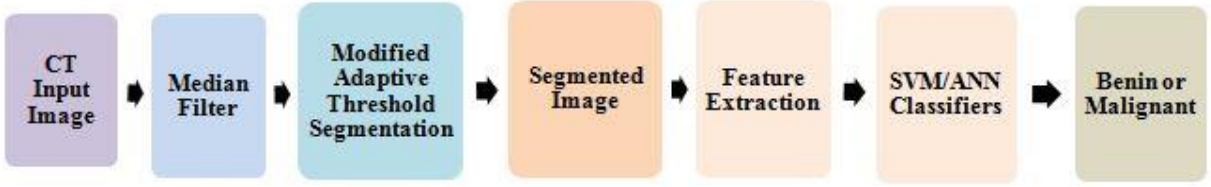

Fig. (1). Block illustration of the suggested method for identifying lung cancer.

2.1. Lung Image Database Consortium (LIDC) and Image Database Resource Initiative (LIDC-IDRI) Dataset

Four exceptionally skilled thoracic radiologists' included lesion annotations throughout the LIDC-IDRI database. 1,018 low-dose lung CT images from 1010 lung patients are included in LIDC-IDRI. Imagery comprising a clinical thoracic CT scan as well as an XML file with the findings of a 2-stage image annotation process completed by four qualified thoracic radiologists have been included for every individual. This collection includes lung cancer screening along with diagnostic thoracic CT pictures with labeled lesions. This is a hub for CAD techniques for lung cancer screening, including diagnostic research, teaching, and assessment.

2.2. Adaptive Threshold Segmentation (ADT) and Modified Adaptive Threshold (ADTM) Segmentation

In its simplest terms, adaptive thresholding converts a color or grayscale visual display into source images that accurately reflect the classification. To implement locally adaptive thresholding, a threshold is calculated for each image pixel individually, which computes the threshold for every pixel to use the local mean intensity all-around pixel's neighborhood with a sensitivity factor defined by sensitivity [52]. Sensitivity is indeed a scalar with a value between 0 and 1 that shows sensitivity to thresholding additional pixels as foreground. Whenever the pixel score is lower than that of threshold values, the foreground score was assumed; however, the background value was calculated. Bradle is another name for this method. This method uses a neighborhood shape that is computed as 2*floor(size(I)/16)+1, which is almost 1/8th the size of the picture. In the Modified Adaptive Threshold, in addition to the Adaptive Threshold method, to remove the outer ring structure or parts of the outer ring structure obtained in some cases, we used a filtering criterion with an assumption that the object's Centroid of Interest lies in the upper 80% of the image.

When it comes to storing, exchanging, and transmitting digital records, the Digital Imaging and Communications in Medicine (DICOM) standards were being universally adopted. DICOM images are often compressed for storage and transmission because they contain multiple high-resolution images. Because of this, they are noisy. So image noise reduction is a must. Median filtering is used because it preserves edges while also reducing noise. By comparing every pixel to its surroundings, a median filter may assess whether a given pixel represents its surroundings. The pixel rate is swapped out for an average of the norms of neighboring pixels. In this case, we choose a 3-by-3-block area. To find the middle value, we rank the neighboring input images numerically and would then replace the target pixel with its median value. If the number of adjacent pixels under examination is even, the center and center pixels of the picture are averaged. The lungs are divided into segments using a technique called modified adaptive threshold. Areas, Center of gravity, Concave Area, Eccentricity, Diameter, Euler Numbers, Extension, Extrema, Minor Axis Long, Major Axis Length, Alignment, Enclosure, and Solidity seem to be just 13 of the many shape features; 7 GLCMs are also available. Contrast, Equilibrium Energy, Homogenisation, Cluster Prominence, Cluster Shade, Dissimilarity, and 8 Intensity are all characteristics of texture. Several statistical parameters are determined, such as the root-mean-square (RMS) variance, central tendency, dispersion, skewness, and inverse difference moment (IDM). Normalized values for the Principal Component Coefficients are calculated by filtering out high and low-intensity features in the Single-Level Discrete 2-D Wavelet Transform.

The classification effectiveness of the predicted methodology parameters of ADT as well as ADTM using ANN and SVM are measured using nine performance metrics, including precision, errors, sensitivities, specificity, false-positive rates, F1 score, Mathews correlation coefficient, as well as kappa-kappa. Cohen's Accuracy could be thought of as the proportion of accurately predicted pixels [53, 54]. The resulting equation is shown below.

$$Acc = (TP + TN)/ (TP + FP + TN + FN)$$

Below, we quantify sensitivity (the fraction of node variables correctly predicted) and accuracy (the fraction of input images correctly predicted).

$$Se = TP/(TP + FN)$$

$$Sp = TN/ (TN + FP)$$

The false negative ratio (FNR) seems to be the proportion of pixels with wrong values, whereas the false positive ratio (FPR) constitutes the proportion of pixels that are mistakenly identified as nodes [25].

$$FPR = FP/(TP + TN)$$

$$FNR = FN /(TP + TN)$$

The overlapping value is an indicator of similarity that is a reproduction of how the principles' subdivision result binds the truth.

$$Overlap = TP/(TP + FP + FN)$$

Where, True-positive (TP) = exactly found number as nodule pixels. False-positive (FP) = incorrect found number as

nodule pixels. True-negative (TN) = the number of exact identifications as background pixels. False Negative (FN) = the number of incorrect identifications as contextual images. Five computation measures have scores ranging from 0 to 1. The better the divisional performance, the lower the FPR as well as FNR.

3. RESULTS AND DISCUSSION

To begin, we must first convert every DICOM image within the LIDC dataset to Jpeg images, after which we can obtain a 534-training dataset and 150-testing database, each of which will feature images of malignant as well as benign tumors of lung cancer. One of the test photographs included in the database is chosen and then converted to grayscale by erasing the color and saturation information while saving the brightness. To increase the quality of the images produced by automatic image processing programs and lessen their reliance on human input, a representativeness reduction technique is employed. Contrast enhancement methods may be divided basically into two groups: those that operate in the frequency domain and those that operate in the spatial domain. Its purpose is to dampen lower frequencies in the frequency domain. Median filtering is utilized during preprocessing because it preserves edges while removing unwanted noise. After each iteration, the filter substitutes every score match with the average for neighboring pixels. Its "window" is simply the configuration of its surrounding pixels, which allows for seamless panning across the entire display. Fig. (**2**) displays the processed photos. The steps in preprocessing are,

Step 1: Initializing a 3×3 Square neighborhood

Step 2: Putting in the numerical arrangement of the pixel data in the immediate area

Step 3: substituting the center pixel value for the one being evaluated.

Step 4: If the number of pixels in the neighborhood under evaluation is even, the sum of its two middle pixel values is utilized.

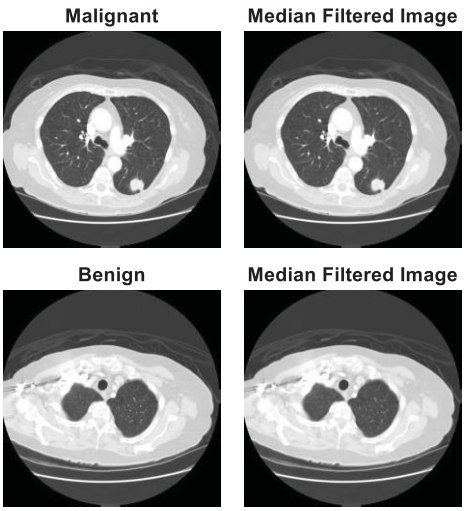

Fig. (2). Median filtered image after preprocessing.

The segmentation of lung images using adaptive thresholding involves the following steps. Initially, it determines the range of global threshold values that can be used to convert an intensity representation toward a binary image. Images are distributed into fragments as component areas or objects. Image subdivision aims to alter an illustration of the image by providing more agreeable results. Because just those pixels with a label may be employed to partition the picture into discrete pieces, it is necessary at this stage to give an identifier to every pixel throughout the image. The most prevalent application of image segmentation is the localization of objects and boundaries in pictures, such as planes and curves. Fig. (**3**) shows a segmented image using the thresholding approach. It shows important information in image segmentation. The benefit of using a threshold is that the segmented image attains less storing space and its dispensation speed increases. The thresholding process is a non-linear operation performed on an image. Grayscale images are transformed in and out of binary ones. The thresholding value assigned to this technique is between 0 and 1. Therefore, the image will be segmented based on threshold values attained on it.

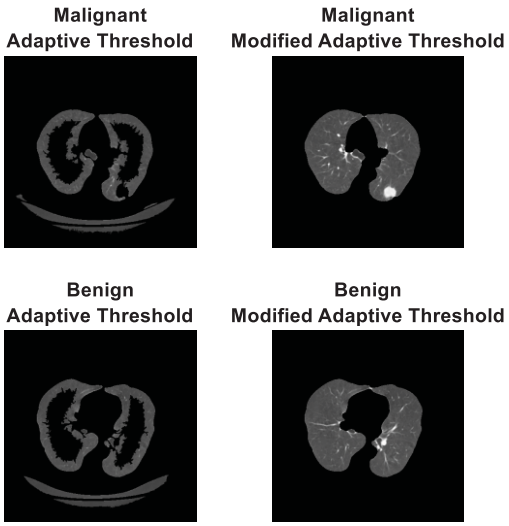

Fig. (3). The output of Adaptive and Modified Adaptive Thresholds for Malignant and Benign images.

The two most common applications of feature extraction are contour recognition as well as image distribution. This characteristic is a recurrent image design. The binarization technique is employed to spot lung cancer as well as isolate the relevant portion of a photograph. The process of feature extraction seems to have been a crucial step in identifying and segmenting a wide variety of predetermined geometries. The amount of grayscale or monochrome pixels is used to determine the degree of binarization. A key part of the binarization architecture is the demonstration that normal tissue images have a significantly greater proportion of black pixels than aberrant lung images with white pixels. An image is considered abnormal if its black-to-white pixel ratio is significantly off the normal range. Binarization is used to obtain the images, as in Fig. (**4**).

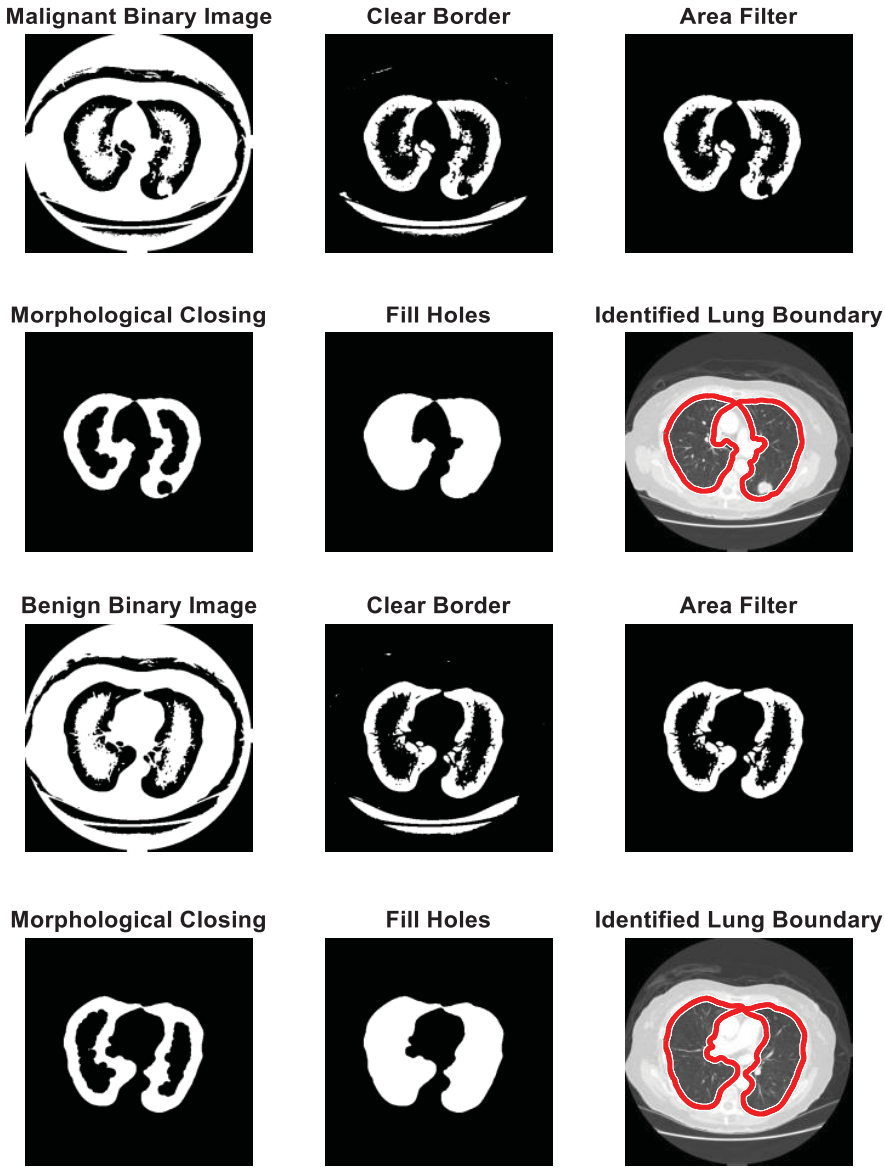

Fig. (4). The binarized, filled output of Benign images, cleared border, and malignant images.

The aforementioned binary images are then subjected to morphological procedures, which degrade binary images by eliminating detail. The next step is to stretch the image to fill in some pixels that would otherwise be invisible from the image's periphery due to their location in the image's context. Finally, a disk-shaped segmentation marker is used to isolate the segmented region in the image pixels.

Grayscale image segmentation can yield a wide variety of useful features; for example, 13 form attributes, 7 GLCM feature descriptors, as well as 8 intensity parameters. These are taken from the basic components that comprise discrete 2-dimensional wavelets with a single degree of granularity. Table **1** displays the 13 retrieved shape features: area, centroid, concave area, eccentricities, equiv dimension, Euler number, extent, extremes, minor and major axis lengths, orientations, perimeter, as well as solidity.

Table **2** lists the seven GLCM indicators that were derived: contrast, stochastic energy, consistency, difference, as well as cluster shade.

Table **3** displays the values for various intensity variables. These include the Standard Deviation, Skewness, Mean, Smoothness, Median, RMS (root-mean-square**)**, Variance, and Kurtosis, as well as IDM (Islanding detection method). The homogeneity of the image affects IDM. IDM will receive small contributions from inhomogeneous areas due to the weighting function. As a consequence, inhomogeneous images have a lower IDM value, whereas homogeneous images have a comparatively greater value. The PCOs of a 1-level discrete 2-dimensional wavelet transform can be utilized to infer intensity characteristics.

Table 1. Segmented regions' shape-based constraints.

S. No.	Parameters	Malignant	Benign
1	Area	23009	16463
2	Centroid	256.643	273.8151
3	ConvexArea	27727.5	23601
4	Eccentricity	0.8263	0.8807
5	EquivDiameter	171.1263	144.7803
6	EulerNumber	1	1
7	Extent	0.6492	0.5317
8	Extrema	248.875	270.75
9	MajorAxisLength	245.7574	255.2849
10	MinorAxisLength	136.5139	120.9415
11	Orientation	-0.8873	-7.0178
12	Perimeter	697.886	764.394
13	Solidity	0.83	0.6976

Table 2. GLCM-based Texture characteristics.

S. No.	GLCM Parameters	Malignant	Benign
1	Contrast	0.0566	0.0314
2	Entropy	0.6445	0.3085
3	Energy	0.6967	0.8786
4	Homogeneity	0.9895	0.9955
5	ClusterProminence	149.2417	31.0958
6	ClusterShade	17.1372	5.5721
7	Dissimilarity	0.0276	0.0129

Table 3. Intensity parameters.

S. No.	Intensity parameters	Malignant	Benign
1	Mean	00.0019	0.0012
2	Standard Deviation	00.0597	0.0587
3	RMS	00.0598	0.0498
4	Variance	00.0036	0.0026
5	Smoothness	00.9732	0.9672
6	Kurtosis	64.4715	78.564
7	Skewness	3.9275	4.752
8	IDM	1.432	3.7424

Measured variables yield a total of 28 characteristics, including 13 contours, 7 GLCM feature descriptors, and 8 intensity characteristics. The above process was done for all the 534 images in the training database, and these features are used for training the designed ANN-based classifier. There are 20 levels in the secret layers. Because of its superior suitability to the present investigation, the log-sigmoid transfer function has been used. The regression map, results, training state, error histogram, and error histogram of the ANN and SVM classifier are depicted in Figs. (**5** to **10**) correspondingly. The training state plot of ANN is shown in Fig. (**5**), and the Error histogram plot of ANN is shown in Fig. (**6**). Based on the obtained label 1 or 2, the output displayed tumor images as benign or malignant, respectively. The regression plot of ANN is shown in Fig. (**7**). The performance plot of ADT and ADTM with ANN is shown in Fig. (**8**). The input image's real label values are determined by utilizing the constructed feed-forward computational model to match it to the pre-existing learned image labels.

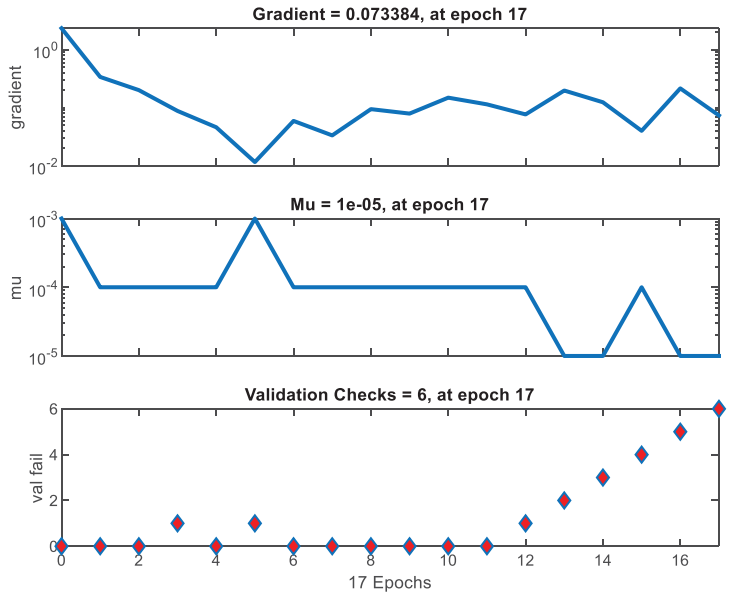

Fig. (5). Training state plot of ANN.

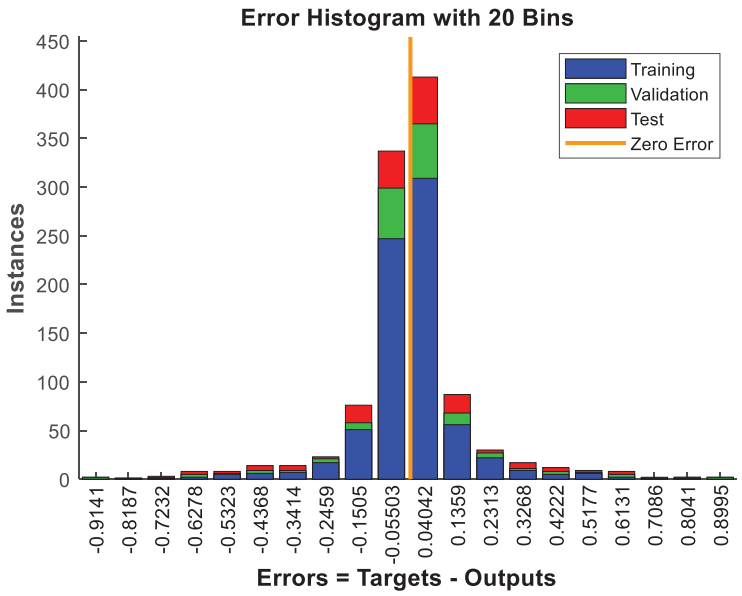

Fig. (6). Error histogram plot of ANN.

According to the results of this research, the optimal number of training iterations for a neural network referred to as epochs in ANN jargon was set to 18. To avoid overfitting, which can occur when the number of iterations is either too low or too high, we designed the network to stop training whenever the best generalization is achieved. This was accomplished by dividing the histograms of directed gradients (HOG) data into three sub-datasets: 70% preparation, 15% validation, and 15% checking. The HOG database was used for conditioning the network, while the reliability of the data set was used to test the network's accuracy. When the fault for the validation dataset began to rise, the network training ended. We also provided the mean square errors (MSE) as well as the accuracy rate for every trial, where the number of hidden neurons varied from 2 - 18 throughout the two phases (from the confusion matrix plot). The MSE is a measure of how far off the output is from the goal. Verification vectors will quickly trigger to terminate training if the network procedure upon that verification matrices keeps on delivering or keeping the same, as evidenced by a rising trend within MSE for validation specimen. We also run a test using a test dataset to see whether the network generalizes well, but this did not impact training. Epoch 17 has the highest accuracy results.

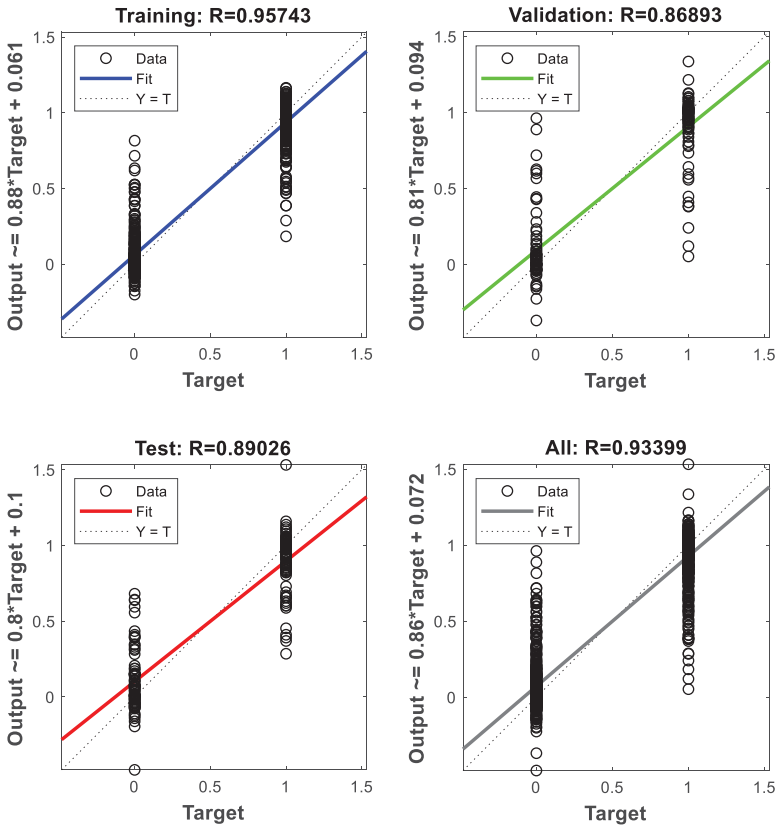

Fig. (7). Regression plot of ANN.

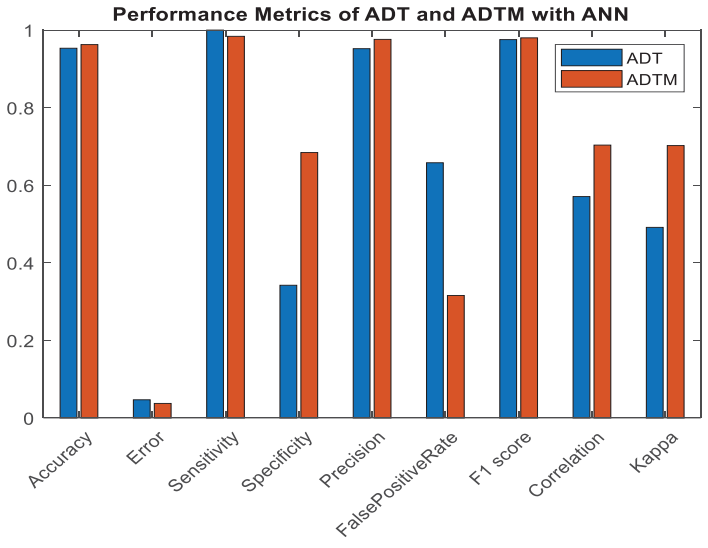

Fig. (8). Performance evaluation of ADT and ADTM with ANN.

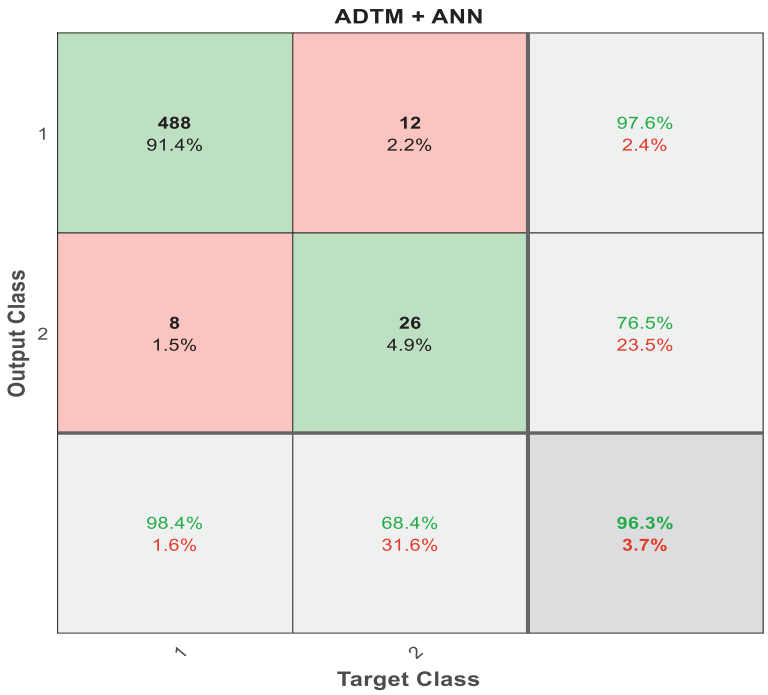

Fig. (9). Confusion Matrices for ADTM with ANN classifier.

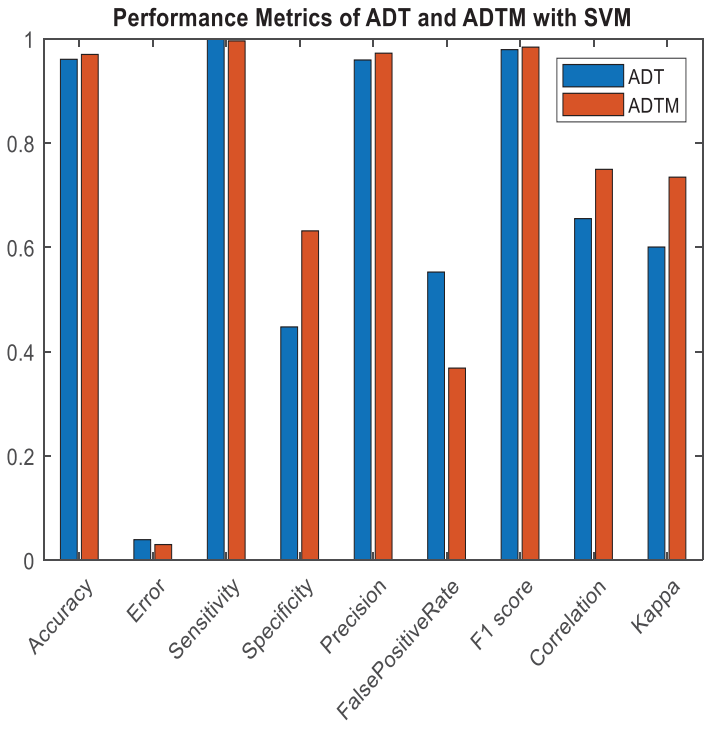

Fig. (10). Performance evaluation with SVM classifier.

Error histogram refers to the distribution of deviations from the predicted value of such a target variable after training a feed-forward neural network. Since they indicate the degree to which actual values deviate from their target counterparts, such error estimates can be negative. The term “bins” describes the range of the graph's vertical lines. There are currently 30 discrete groups within the higher error spectra. Upon that Y-axis, we can see the percentage of the whole dataset that fits through every bin [53]. Fig. (**6**) displays the theoretical network's error histogram, which displays how the error scales

are distributed. To evaluate the results, the terms Sensitivity (SE), Accuracy (AC), and Specificity (SP) are employed. The diagnostic accuracy of a test is measured by its sensitivity. The capacity of a test to definitively exclude a potential outcome is known as its "specificity." The number of observations correctly categorized determines classification accuracy. The regression plot of network outputs concerning preparation, research, validation and test sets is shown in Fig. (**7**). A straight line represents the best-fit linear regression line between outcomes and aims. The correlation between several outputs and the targets is denoted by R, where R=1 indicates a perfect match. To put it another way, if R=0, there will be no connection between outcomes and objectives.

Multiple classes are labeled and predicted to generate a confusion matrix [55]. a False Positive (FP), A True Positive (TP), a True Negative (TN), and a False Negative (FN) are all possible outcomes in the Two-Class of Confusion Matrix. Accuracy, error, Sensitivity (Recall or TP rate), Specificity, Precision, FPR-FP rate, F1 score, MCC-Matthews correlation coefficient, and kappa-kappa Cohen's are calculated to evaluate the accuracy of ADT and ADTM using ANN, as illustrated in (Fig. **1** and Table **4**).

The rows of the multiplication chart, including a confusion matrix, stand for the target domain (Output Class), whereas the bars stand for the class label themselves (Target Class). Accurate particulars are represented by the cells along that diagonal. The labels above the off-diagonal cells that correspond to the breakthroughs are wrong. Uncertainty matrices display the relative frequency of right and wrong categories. Appropriate classifications are represented by green squares upon that diagonally of said matrices and wrong ones by red squares. Distinct cells demonstrate the percentage of the overall observations that can be interpreted, as well as the entire amount of explanations. Columns on the far side of both maps indicate what percentage of expected occurrences was correctly and incorrectly labeled. Among the most common criteria used was the percentage of false positives or accuracy (or positive predictive score). The line at the bottom of the graph displays the percentage of successfully and incorrectly classified cases across all anticipated classes. Two metrics that saw frequent use are recalled (called true +ve rate and false -ve rate). The accuracy is represented by the number of white cells in the bottom right portion of the map.

In Fig. (**9**), the confusion matrix with targeted and output classes is indicated. The number and percentage of successfully replicated arrangements using the trained system are displayed in the top two diagonal cells. Only 488 images out of 534 could be confidently labeled as benign (the true positive). Nearly ninety-two percent of the 534 photographs are compared to show similarity. To the same extent, 12 instances are accurately diagnosed as malignant (true negative). Only 2.2% of all photos can be distinguished from this. A false-positive rate of 1.5% was achieved when 8 malignant imageries were misclassified as benign. Also, 4.9% of all data, or 26 benign images, are misclassified as cancerous (False negative). With the ANN classifier, ADTM achieves an impressive 96.3% accuracy with a margin of error of only 3.7%.

Table 4. Performance analysis of ADT and ADTM using ANN.

S. No.	Performance Analysis	ADT	ADTM
1	Accuracy	95.3184	96.2547
2	Error	4.6816	3.7453
3	Sensitivity	99.9999	98.3871
4	Specificity	34.2105	68.4211
5	Precision	95.2015	97.6
6	False positive rate	65.7895	31.5789
7	F1_score	97.5418	97.992
8	Mathews Correlation Coefficient	57.0692	70.3457
9	Kappa	49.1351	70.2208

Table 5. Evaluation Metrics of ADT & ADTM using SVM classifier.

S. No.	Performance Analysis	ADT	ADTM
1	Accuracy	96.0674	97.0037
2	Error	3.9326	2.9963
3	Sensitivity	99.9999	99.5968
4	Specificity	44.7368	63.1579
5	Precision	95.9381	97.2441
6	False positive rate	55.2632	36.8421
7	F1_score	97.9269	98.4064
8	Mathews Correlation Coefficient	65.5131	74.9653
9	Kappa	60.0613	73.4658

The results of an SVM classifier performance analysis are displayed in (Table **5** and Fig. **10**). Most 97.00% total accuracy is better than that of the other classifiers studied for this paper by a wide margin. Since SVM is less sensitive to the sample and uses only support vectors to create the separating hyperplane, a rise in the number of training specimens had little effect on accuracy.

Fig. (**11**) shows the ADTM-SVM confusion matrix with the input class and the expected output class. Only 494 of the 534 photos can be safely classified as malignant, the true positive. Almost 93% of the 534 photographs on the site have some similarity to this. In a similar vein, 14 cases met the criteria for malignancy (true negative). To be exact, it is similar to 2.6% of all photos. Two photos are misclassified as false positive (as benign), or 0.4%. Conversely, 4.5% of the total data corresponds to 24 benign photos wrongly classified as cancer (False negative). ADTM using an SVM classifier, achieves 97.0% accuracy with a 3.0% margin of error. Classification models combining depth features, radiomics features, and multi-scale features are compared and depicted in Table **6**.

To properly examine the impact of every single component within the suggested investigation, we conducted extensive ablation procedures using 7 training alongside two testing groups [64 - 66]. Table **7** compares our results from using classifiers with those from not using them when screening for ADT and ADTM.

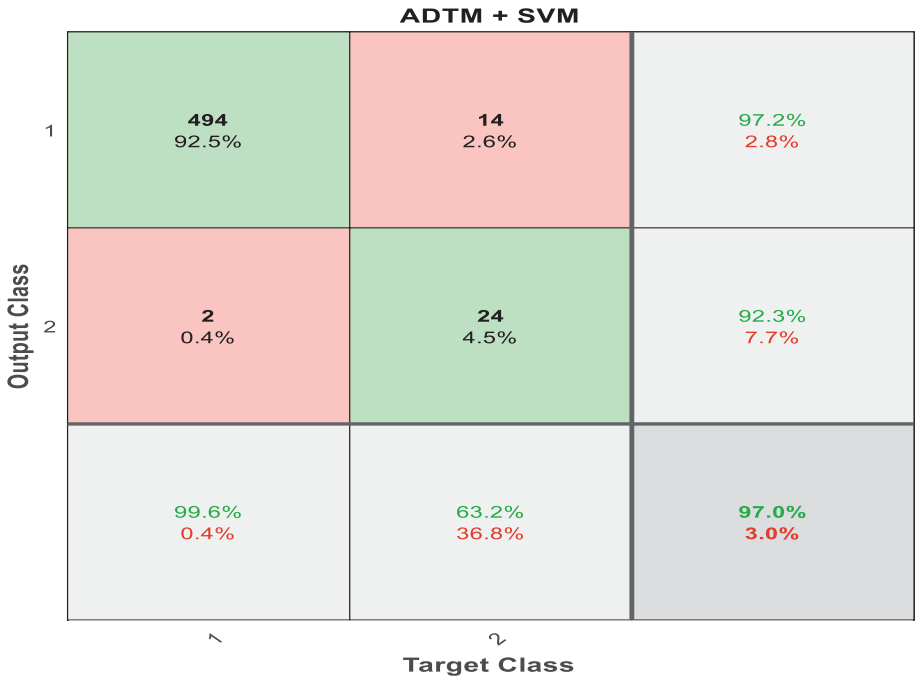

Fig. (11). Confusion Matrix for ADTM with SVM.

Table 6. Analysis of various classification models.

Reference No.	Type	Sensitivity	Specificity	Accuracy
[56]	Combinational features	73.70	95.40	83.20
[57]	Hybrid model	78.80	87.90	93.80
[58]	Radiomics + CNN	97.00	88.00	89.00
[59]	Hybrid model	78.00	88.00	85.00
[60]	Multi-scale approach	79.43	93.76	87.65
[61]	Multi-feature CNN	91.00	89.00	92.00
[62]	CNN (n-ClsNet)	93.78	90.14	93.80
[63]	Multi-feature multi-scale CNN	85.00	94.00	90.00
-	Proposed (ADTM+ANN)	98.3871	68.4211	96.25
-	Proposed (ADTM+SVM)	99.5968	63.1579	97.00

Table 7. Evaluation using parameters of ADT & ADTM with and without classifiers.

S. No.	Features	ADT	ADTM	ADT + ANN	ADTM + ANN	ADT + SVM	ADTM + SVM
1	Accuracy	54.21	76.32	95.3184	96.2547	96.0674	97.0037
2	Error	6.36	5.95	4.6816	3.7453	3.9326	2.9963
3	Sensitivity	52.18	69.68	99.9999	98.3871	99.9999	99.5968
4	Specificity	56.94	73.77	34.2105	68.4211	44.7368	63.1579
5	Precision	54.00	75.48	95.2015	97.6	95.9381	97.2441
6	False positive rate	45.97	52.56	65.7895	31.5789	55.2632	36.8421

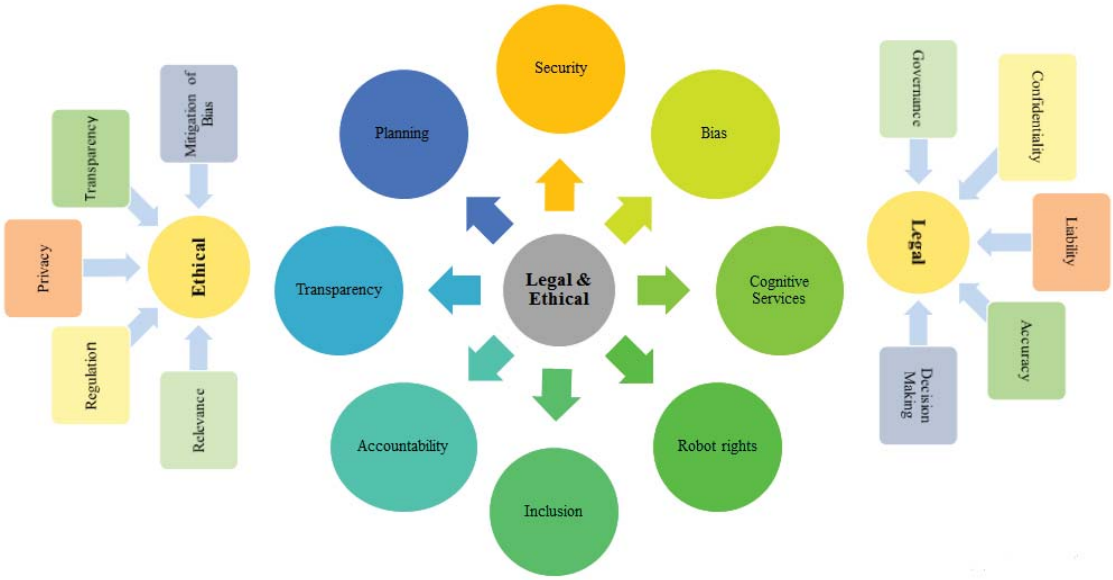

Fig. (12). Ethical and legal considerations in AI.

The systems use ANN as well as SVM, two types of intelligent classifiers that have proven effective in separating benign from malignant lung tumors. The primary goal of this study is to refine existing image-processing methods for segmenting lung tumors into discrete regions. The suggested methods for automated lung tumor segmentation using CT images are easy to implement yet potentially play an important role in modern medicine. The suggested method provides the best possible option for rapidly and accurately diagnosing lung cancer. As a result, the proposed system employs sophisticated image processing methods like thresholding in an easy-to-use framework to facilitate cancer detection. Numerous affected and unaffected images from an online database are used to evaluate the developed system. The goal of the tests was to prove that the suggested system could successfully detect lung tumors without human intervention and pave the way for early diagnosis.

3.1. Ethical Issues Regarding Artificial Intelligence (AI) and Machine Learning (ML) in Medical Diagnosis

Due to advances in computing, the reasoning process underpinning Artificial Intelligent System (AIS) results may be obscured, rendering in-depth analysis impractical. Adopting AI to assist clinicians in the future may result in a shift in stakeholder dynamics and clinical decision-making [67]. Using AIS in the future to aid clinicians possess the capability to completely alter the healthcare system if it is extensively adopted. Safe use of novel technology within clinical settings is crucial to clinicians. Since robot physicians and nurses lack human characteristics, such as compassion, their interactions with patients will be less empathic, considerate, and appropriate [68]. This is arguably the most severe drawback of AI in the medical field. Artificial intelligence in healthcare needs to be flexible enough to respond to novel situations while maintaining ethical standards. AIS can have sudden and dramatic failures when the environment or conditions change [69]. In a single second, AI may go from extremely savvy to extremely naïve. The ethical and legal consideration of AI is shown in Fig. (**12**).

It is important to ensure the human decision-maker makes the choices and that the machine understands and can work within the restrictions of the structure of the system. Whenever a medical diagnosis and therapy system is mostly accurate, doctors using it may get complacent as well as stop learning new things or enjoying their work [70]. Moreover, individuals may accept the results of a decision support system without considering their limitations. Similarly, there are legitimate cyber security risks with the usage of AI with no human intervention. In contrast to medical professionals, technologists

are not held legally accountable for their actions; instead, the profession relies on the application of ethical standards of conduct [71]. This metaphor well captures the core of the discussion about accountability for the adverse effects of AIS implementation in healthcare settings. Considerations about patient safety rise when AISs used in clinical settings aren't currently evaluated or verified. This aspect of technology is indeed challenging to master. Despite the need for a new approvals framework and strategy for AI systems, the ultimate responsibility for their use remains with the qualified professionals and hospitals that employ them. AI-based medical devices will assist individuals in making treatment and procedure decisions, as opposed to replacing them entirely. As our dependence on it grows, we must ensure that judgments made by AI are impartial and free of prejudice. Transparent, accessible, and accountable AI systems are the only way forward. The usage of AI systems is on the rise in the field of medicine, where they are surpassing people by bettering patient paths and surgical results. It is expected that AI will either complement, coexist alongside or replace existing medical systems.

CONCLUSION

In comparison to other types of tumors, the fatality rate is highest for lung cancer. In this research, images are processed and classified to arrive at a diagnosis. The nodes are identified, and certain characteristics have been removed using these measures. The derived characteristics are used to classify disease stages. The phases of lung tumors are classified employing a feed-forward neural network. This innovation may have a major impact on the worldwide rate of lung cancer rate due to its ability to detect lung tumors in their earliest stages when they are most amenable to being avoided and treated. This method is useful because it provides more information and facilitates quick and precise decision-making for doctors diagnosing lung cancer in their patients. The suggested approach for lung cancer diagnosis only with the ANN classifier has an accuracy of 96.3%, while the SVM classifier has an accuracy of 97%; this suggests that the SVM classifier offers high accuracy using ADTM in lung tumor classification. Moreover, both the ANN and SVM classifiers used in the suggested technique for lung cancer diagnosis achieve world-record levels of accuracy.

LIST OF ABBREVIATIONS

SVM	=	Support Vector Machines
ANN	=	Artificial Neural Network
LIDC	=	Lung Image Database Consortium
CT	=	Computed Tomography
IDM	=	Islanding Detection Method
ADT	=	Adaptive Threshold Segmentation

ETHICS APPROVAL AND CONSENT TO PARTICIPATE

Not applicable.

HUMAN AND ANIMAL RIGHTS

The studies utilized as the foundation for this study did not involve the use of any animals or people.

CONSENT FOR PUBLICATION

Not applicable.

AVAILABILITY OF DATA AND MATERIALS

The data and supportive information are available within the article.

FUNDING

None.

CONFLICT OF INTEREST

The authors declare no conflict of interest financial or otherwise.

ACKNOWLEDGEMENTS

The authors would like to thank the Noorul Islam Centre for Higher Education's Physics Department for their assistance.

REFERENCES

[1] Society C. Cancer facts and figures. Atlanta: American Cancer Society 2013.

[2] Cancer Facts and Figures. 2017. Available from: https://www.cancer.org/research/cancer-facts-statistics/all-cancer-facts-figures/cancer-facts-figures-2017.html

[3] Hansell DM, Bankier AA, MacMahon H, McLoud TC, Müller NL, Remy J. Fleischner Society: Glossary of terms for thoracic imaging. Radiology 2008; 246(3): 697-722. [http://dx.doi.org/10.1148/radiol.2462070712] [PMID: 18195376]

[4] Valente IRS, Cortez PC, Neto EC, Soares JM, de Albuquerque VHC, Tavares JMRS. Automatic 3D pulmonary nodule detection in CT images: A survey. Comput Methods Programs Biomed 2016; 124: 91-107. [http://dx.doi.org/10.1016/j.cmpb.2015.10.006] [PMID: 26652979]

[5] Lee SLA, Kouzani AZ, Hu EJ. Automated detection of lung nodules in computed tomography images: A review. Mach Vis Appl 2012; 23(1): 151-63. [http://dx.doi.org/10.1007/s00138-010-0271-2]

[6] Armato SG III, Meyer CR, McNitt-Gray MF, *et al.* The Reference Image Database to Evaluate Response to therapy in lung cancer (RIDER) project: A resource for the development of change-analysis software. Clin Pharmacol Ther 2008; 84(4): 448-56. [http://dx.doi.org/10.1038/clpt.2008.161] [PMID: 18754000]

[7] McNitt-Gray MF, Armato SG III, Meyer CR, Reeves AP, McLennan G, Pais RC, *et al.* The LIDC(LIDC) data collection process for nodule detection and annotation. Acad Radiol 2007; 14(12): 1464-74. [http://dx.doi.org/10.1016/j.acra.2007.07.021] [PMID: 18035276]

[8] Public Lung Image Database. Available from: http://www.via.cornell.edu/lungdb.html

[9] Cascio D, Magro R, Fauci F, Iacomi M, Raso G. Automatic detection of lung nodules in CT datasets based on stable 3D mass–spring models. Comput Biol Med 2012; 42(11): 1098-109. [http://dx.doi.org/10.1016/j.compbiomed.2012.09.002] [PMID: 23020972]

[10] Soltaninejad S, Keshani M, Tajeripour F. Lung nodule detection by KNN classifier and active contour modelling and 3D visualization. The 16th CSI International Symposium on Artificial Intelligence and Signal Processing (AISP 2012). 440-5.

[11] Kim H, Nakashima T, Itai Y, Maeda S. Automatic detection of ground glass opacity from the thoracic MDCT images by using density features. 2007 International Conference on Control, Automation and Systems. 1274-7.

[12] Pu J, Roos J, Yi CA, Napel S, Rubin GD, Paik DS. Adaptive border marching algorithm: Automatic lung segmentation on chest CT

images. Comput Med Imaging Graph 2008; 32(6): 452-62. [http://dx.doi.org/10.1016/j.compmedimag.2008.04.005] [PMID: 18515044]

[13] Gori I, Bellotti R, Cerello P, Cheran SC, De Nunzio G, Fantacci ME. Lung nodule detection in screening computed tomography. 2006 IEEE Nuclear Science Symposium Conference Record 2006; 6: 3489-91.

[14] Wei GQ, Fan L, Qian J. Automatic detection of nodules attached to vessels in lung CT by volume projection analysis. International Conference on Medical Image Computing and Computer-Assisted Intervention. 746-52. [http://dx.doi.org/10.1007/3-540-45786-0_92]

[15] Retico A, Delogu P, Fantacci ME, Gori I, Preite Martinez A. Lung nodule detection in low-dose and thin-slice computed tomography. Comput Biol Med 2008; 38(4): 525-34. [http://dx.doi.org/10.1016/j.compbiomed.2008.02.001] [PMID: 18342844]

[16] Namin ST, Moghaddam HA, Jafari R, Esmaeil-Zadeh M, Gity M. Automated detection and classification of pulmonary nodules in 3D thoracic CT images. 2010 IEEE International Conference on Systems, Man and Cybernetics. 3774-9. [http://dx.doi.org/10.1109/ICSMC.2010.5641820]

[17] Choi WJ, Choi TS. Automated pulmonary nodule detection based on three-dimensional shape-based feature descriptor. Comput Methods Programs Biomed 2014; 113(1): 37-54. [http://dx.doi.org/10.1016/j.cmpb.2013.08.015] [PMID: 24148147]

[18] Keshani M, Azimifar Z, Tajeripour F, Boostani R. Lung nodule segmentation and recognition using SVM classifier and active contour modeling: A complete intelligent system. Comput Biol Med 2013; 43(4): 287-300. [http://dx.doi.org/10.1016/j.compbiomed.2012.12.004] [PMID: 23369568]

[19] Kim DY, Kim JH, Noh SM, Park JW. Pulmonary nodule detection using chest CT images. Acta Radiol 2003; 44(3): 252-7. [http://dx.doi.org/10.1080/j.1600-0455.2003.00061.x] [PMID: 12751994]

[20] Bellotti R, De Carlo F, Gargano G, *et al.* A CAD system for nodule detection in low-dose lung CTs based on region growing and a new active contour model. Med Phys 2007; 34(12): 4901-10. [http://dx.doi.org/10.1118/1.2804720] [PMID: 18196815]

[21] El-Baz A, Elnakib A, Abou El-Ghar M, Gimel'farb G, Falk R, Farag A. Automatic detection of 2D and 3D lung nodules in chest spiral CT scans. Int J Biomed Imaging 2013; 2013: 1-11. [http://dx.doi.org/10.1155/2013/517632] [PMID: 23509444]

[22] Suiyuan W, Junfeng W. Pulmonary nodules 3D detection on serial CT scans. 2012 Third Global Congress on Intelligent Systems. 257-60. [http://dx.doi.org/10.1109/GCIS.2012.46]

[23] Xu N, Ahuja N, Bansal R. Automated lung nodule segmentation using dynamic programming and EM-based classification. Medical Imaging 2002: Image Processing International Society for Optics and Photonics 2002; 4684: 666-76.

[24] Aoyama M, Li Q, Katsuragawa S, Li F, Sone S, Doi K. Computerized scheme for determination of the likelihood measure of malignancy for pulmonary nodules on low-dose CT images. Med Phys 2003; 30(3): 387-94. [http://dx.doi.org/10.1118/1.1543575] [PMID: 12674239]

[25] Wang J, Engelmann R, Li Q. Segmentation of pulmonary nodules in three-dimensional CT images by use of a spiral-scanning technique. Med Phys 2007; 34(12): 4678-89. [http://dx.doi.org/10.1118/1.2799885] [PMID: 18196795]

[26] Fan L, Qian J, Odry BL, *et al.* Automatic segmentation of pulmonary nodules by using dynamic 3D cross-correlation for interactive CAD systems. Medical Imaging 2002: Image Processing International Society for Optics and Photonics 2002; 4684: 1362-9.

[27] Kostis WJ, Reeves AP, Yankelevitz DF, Henschke CI. Three-dimensional segmentation and growth-rate estimation of small pulmonary nodules in helical CT images. IEEE Trans Med Imaging 2003; 22(10): 1259-74. [http://dx.doi.org/10.1109/TMI.2003.817785] [PMID: 14552580]

[28] Enquobahrie AA, Reeves AP, Yankelevitz DF, Henschke CI. Automated detection of pulmonary nodules from whole lung helical CT scans: Performance comparison for isolated and attached nodules. Medical Imaging 2004: Image Processing International Society for Optics and Photonics 2004; 5370: 791-800.

[29] Li Q, Li F, Doi K. Computerized detection of lung nodules in thin-section CT images by use of selective enhancement filters and an automated rule-based classifier. Acad Radiol 2008; 15(2): 165-75. [http://dx.doi.org/10.1016/j.acra.2007.09.018] [PMID: 18206615]

[30] Kawata Y, Niki N, Ohmatsu H, Kusumoto M, Kakinuma R, Mori K. Hybrid classification approach of malignant and benign pulmonary nodules based on topological and histogram features. International Conference on Medical Image Computing and Computer-Assisted Intervention. 297-306. [http://dx.doi.org/10.1007/978-3-540-40899-4_30]

[31] Matsumoto S, Kundel HL, Gee JC, Gefter WB, Hatabu H. Pulmonary nodule detection in CT images with quantized convergence index filter. Med Image Anal 2006; 10(3): 343-52. [http://dx.doi.org/10.1016/j.media.2005.07.001] [PMID: 16542867]

[32] Jia T, Zhao DZ, Yang JZ, Wang X. Automated detection of pulmonary nodules in HRCT images. 2007 1st International Conference on Bioinformatics and Biomedical Engineering. 833-6.

[33] Fukano G, Takizawa H, Shigemoto K, *et al.* Recognition method of lung nodules using blood vessel extraction techniques and 3D object models. Medical Imaging 2003: Image Processing International Society for Optics and Photonics 2003; 5032: 190-8.

[34] Zhao L, Boroczky L, Lee KP. False positive reduction for lung nodule CAD using support vector machines and genetic algorithms. In: International Congress Series. 2005; 1281: pp. 1109-14. [http://dx.doi.org/10.1016/j.ics.2005.03.061]

[35] Dehmeshki J, Chen J, Casique MV, Karakoy M. Classification of lung data by sampling and support vector machine. Conf Proc IEEE Eng Med Biol Soc 2004; 2004: 3194-7.

[36] Santos AM, de Carvalho Filho AO, Silva AC, de Paiva AC, Nunes RA, Gattass M. Automatic detection of small lung nodules in 3D CT data using Gaussian mixture models, Tsallis entropy and SVM. Eng Appl Artif Intell 2014; 36: 27-39. [http://dx.doi.org/10.1016/j.engappai.2014.07.007]

[37] Matsumoto S, Ohno Y, Yamagata H, Takenaka D, Sugimura K. Computer-aided detection of lung nodules on multidetector row computed tomography using three-dimensional analysis of nodule candidates and their surroundings. Radiat Med 2008; 26(9): 562-9. [http://dx.doi.org/10.1007/s11604-008-0272-5] [PMID: 19030967]

[38] Al-Tarawneh MS. Lung cancer detection using image processing techniques. Leonardo J Pract Technol 2012; 11(20): 147-58.

[39] Chaudhary A, Singh SS. Lung cancer detection on CT images by using image processing. 2012 International Conference on Computing Sciences. 142-6. [http://dx.doi.org/10.1109/ICCS.2012.43]

[40] Hadavi N, Nordin MJ, Shojaeipour A. Lung cancer diagnosis using CT-scan images based on cellular learning automata. 2014 International Conference on Computer and Information Sciences (ICCOINS). 1-5. [http://dx.doi.org/10.1109/ICCOINS.2014.6868370]

[41] Aggarwal T, Furqan A, Kalra K. Feature extraction and LDA based classification of lung nodules in chest CT scan images. 2015 International Conference on Advances in Computing, Communications and Informatics (ICACCI). 1189-93. [http://dx.doi.org/10.1109/ICACCI.2015.7275773]

[42] Bhat G, Biradar V G, Sarojadevi H. Artificial Neural Network based Cancer Cell Classification (ANN–C3). 2012.

[43] Pathan A, Saptalkar BK. Detection and classification of lung cancer using artificial neural network. International Journal on Advanced Computer Engineering and Communication Technology 2012; 1(1)

[44] Lin DT, Yan CR. Lung nodules identification rules extraction with neural fuzzy network. Proceedings of the 9th International Conference on Neural Information Processing, 2002 ICONIP'02. 4: 2049-53.

[45] Zhao B, Gamsu G, Ginsberg M S, Jiang L, Schwartz L H. Automatic detection of small lung nodules on CT utilizing a local density maximum algorithm. J Appl Clin Med Phys 2003; 4(3): 248-60.

[46] El-Bazl A, Farag AA, Falk R, La Rocca R. Automatic identification of lung abnormalities in chest spiral CT scans. 2003 IEEE International Conference on Acoustics, Speech, and Signal Processing, 2003 Proceedings (ICASSP'03). 2: 261.

[47] Van Ginneken B, Ter Haar Romeny BM, Viergever MA. Computer-aided diagnosis in chest radiography: A survey. IEEE Trans Med Imaging 2001; 20(12): 1228-41. [http://dx.doi.org/10.1109/42.974918] [PMID: 11811823]

[48] Joon P, Jatain A, Bhaskar SB. Lung cancer detection using image processing techniques: Review. Int J Eng Sci Sci & Comp 2017; 7(4)

[49] Sharma D, Jindal G. Identifying lung cancer using image processing techniques. International Conference on Computational Techniques and Artificial Intelligence (ICCTAI). 17: 872-80.

[50] ullah M, Bari M, Ahmed A, Naveed S. Lung cancer detection using digital image processing techniques: A review. Mehran Univ Res J Eng Technol 2019; 38(2): 351-60.

[http://dx.doi.org/10.22581/muet1982.1902.10]
[51] Ada RK. Early detection and prediction of lung cancer survival using neural network classifier. Int J Appl Innov Eng Manag 2013; 2(6)
[52] Masud M, Sikder N, Nahid AA, Bairagi AK, AlZain MA. A machine learning approach to diagnosing lung and colon cancer using a deep learning-based classification framework. Sensors 2021; 21(3): 748. [http://dx.doi.org/10.3390/s21030748] [PMID: 33499364]
[53] Zheng Q, Yang L, Zeng B, *et al.* Artificial intelligence performance in detecting tumor metastasis from medical radiology imaging: A systematic review and meta-analysis. E Clinical Medicine 2021; 31: 100669. [http://dx.doi.org/10.1016/j.eclinm.2020.100669] [PMID: 33392486]
[54] Maleki N, Zeinali Y, Niaki STA. A k-NN method for lung cancer prognosis with the use of a genetic algorithm for feature selection. Expert Syst Appl 2021; 164: 113981. [http://dx.doi.org/10.1016/j.eswa.2020.113981]
[55] Ito H, Suzuki K, Mizutani T, *et al.* Long-term survival outcome after lobectomy in patients with clinical T1 N0 lung cancer. J Thorac Cardiovasc Surg 2021; 161(1): 281-90. [http://dx.doi.org/10.1016/j.jtcvs.2019.12.072] [PMID: 32067786]
[56] Ning Z, Luo J, Li Y, Han S, Feng Q, Xu Y. Pattern classification for gastrointestinal stromal tumors by integration of radiomics and deep convolutional features. IEEE J Biomed Health Inform 2019; 23(3): 1181-91. [PMID: 29993591]
[57] Choi YS, Bae S, Chang JH, *et al.* Fully automated hybrid approach to predict the *IDH* mutation status of gliomas *via* deep learning and radiomics. Neuro-oncol 2021; 23(2): 304-13. [http://dx.doi.org/10.1093/neuonc/noaa177] [PMID: 32706862]
[58] Calabrese E, Rudie JD, Rauschecker AM, *et al.* Combining radiomics and deep convolutional neural network features from preoperative MRI for predicting clinically relevant genetic biomarkers in glioblastoma. Neurooncol Adv 2022; 4(1): vdac060. [http://dx.doi.org/10.1093/noajnl/vdac060] [PMID: 35611269]
[59] Huang W, Wang J, Wang H, *et al.* PET/CT based EGFR mutation status classification of NSCLC using deep learning features and radiomics features. Front Pharmacol 2022; 13: 898529. [http://dx.doi.org/10.3389/fphar.2022.898529] [PMID: 35571081]
[60] Vuong TTL, Song B, Kim K, Cho YM, Kwak JT. Multi-scale binary pattern encoding network for cancer classification in pathology images. IEEE J Biomed Health Inform 2022; 26(3): 1152-63. [http://dx.doi.org/10.1109/JBHI.2021.3099817] [PMID: 34310334]
[61] Ning Z, Tu C, Xiao Q, Luo J, Zhang Y. Multi-scale gradational-order fusion framework for breast lesions classification using ultrasound images. Medical Image Computing and Computer Assisted Intervention–MICCAI 2020: 23rd International Conference, Lima, Peru, October 4–8, 2020 2020; 23(Part VI): 171-80.
[62] Wang L, Zhou X, Nie X, *et al.* A multi-scale densely connected convolutional neural network for automated thyroid nodule classification. Front Neurosci 2022; 16: 878718. [http://dx.doi.org/10.3389/fnins.2022.878718] [PMID: 35663553]
[63] Che H, Brown LG, Foran DJ, Nosher JL, Hacihaliloglu I. Liver disease classification from ultrasound using multi-scale CNN. Int J CARS 2021; 16(9): 1537-48. [http://dx.doi.org/10.1007/s11548-021-02414-0] [PMID: 34097226]
[64] Dou Q, Chen H, Jin Y, Lin H, Qin J, Heng PA. Automated pulmonary nodule detection *via* 3d convnets with online sample filtering and hybrid-loss residual learning. Medical Image Computing and Computer Assisted Intervention− MICCAI 2017: 20th International Conference, Quebec City, QC, Canada, September 11-13, 2017, Proceedings, Part III 20. 630-8.
[65] Chui KT, Gupta BB, Jhaveri RH, *et al.* Multiround Transfer Learning and Modified Generative Adversarial Network for Lung Cancer Detection. Int J Intell Syst 2023; 2023: 1-14. [http://dx.doi.org/10.1155/2023/6376275]
[66] Chan MV, Huo YR, Cao C, Ridley L. Survival outcomes for surgical resection *versus* CT-guided percutaneous ablation for stage I non-small cell lung cancer (NSCLC): A systematic review and meta-analysis. Eur Radiol 2021; 31(7): 5421-33. [http://dx.doi.org/10.1007/s00330-020-07634-7] [PMID: 33449192]
[67] Naik N, Hameed BMZ, Shetty DK, *et al.* Legal and ethical consideration in artificial intelligence in healthcare: Who takes responsibility? Front Surg 2022; 9: 862322. [http://dx.doi.org/10.3389/fsurg.2022.862322] [PMID: 35360424]
[68] Iqbal MJ, Javed Z, Sadia H, *et al.* Clinical applications of artificial intelligence and machine learning in cancer diagnosis: Looking into the future. Cancer Cell Int 2021; 21(1): 270. [http://dx.doi.org/10.1186/s12935-021-01981-1] [PMID: 34020642]
[69] Ienca M, Ignatiadis K. Artificial intelligence in clinical neuroscience: methodological and ethical challenges. AJOB Neurosci 2020; 11(2): 77-87. [http://dx.doi.org/10.1080/21507740.2020.1740352] [PMID: 32228387]
[70] Higgins O, Short BL, Chalup SK, Wilson RL. Artificial intelligence (AI) and machine learning (ML) based decision support systems in mental health: An integrative review. Int J Ment Health Nurs 2023; inm.13114. [http://dx.doi.org/10.1111/inm.13114] [PMID: 36744684]
[71] Shreve JT, Khanani SA, Haddad TC. Artificial intelligence in oncology: Current capabilities, future opportunities, and ethical considerations. Am Soc Clin Oncol Educ Book 2022; 42(42): 842-51. [http://dx.doi.org/10.1200/EDBK_350652] [PMID: 35687826]